Supplement of Atmos. Chem. Phys., 26, 7867–7894, 2026
https://doi.org/10.5194/acp-26-7867-2026-supplement

Atmospheric Chemistry and Physics
Open Access
EGU

Supplement of

Impacts of lake on diurnal evolution of surface $PM_{2.5}$ concentrations around a typical megacity of China

Zining Yang et al.

Correspondence to: Qike Yang (yangqike@ustc.edu.cn)

Contents of this file

Figure S10: The spatial distribution of secondary $PM_{2.5}$ near-surface concentrations in the Lake experiment and the differences between Lake and Nolake experiments.

Figure S11: The vertical cross-section of $PM_{2.5}$ concentration and wind vectors along the key path AC for the Lake experiment, Nolake experiment, and their differences.

Figure S12: The vertical profiles of $PM_{2.5}$ concentrations simulated in the Lake experiment, Nolake experiment, and their differences over urban and lake regions.

Figure S13: The spatial distribution of 10-m wind speed in the Lake experiment, Nolake experiment, and their differences.

Figure S14: The vertical cross-section of chemical process contributions to $PM_{2.5}$ concentrations during nighttime along the key path AC for the Lake experiment, Nolake experiment, and their differences.

Figure S15: The vertical cross-section of chemical process contributions to $PM_{2.5}$ concentrations at 08:00 and 14:00 LT along the key path AC for the Lake experiment, Nolake experiment, and their differences.

Figure S16: The spatial distribution of NO_3^- near-surface concentrations in the Lake experiment and the differences between Lake and Nolake experiments.

Figure S17: The spatial distribution of NH_4^+ near-surface concentrations in the Lake experiment and the differences between Lake and Nolake experiments.

Figure S18: The spatial distribution of SO_4^{2-} near-surface concentrations in the Lake experiment and the differences between Lake and Nolake experiments.

Figure S19: The spatial distribution of $PM_{2.5}$ near-surface concentrations in the Lake_emis experiment and the differences between Lake_emis and Nolake_emis experiments.

Figure S20: The vertical cross-section of $PM_{2.5}$ concentration and wind vectors along the key path AC for the Lake_emis experiment, Nolake_emis experiment, and their differences.

Table S1. Description of land cover data classifications

Number	Description
1	Urban
2	Dryland cropland/pasture
3	Irrigated cropland/pasture
4	Mixed Dryland/Irrigated Cropland
5	Cropland/Grassland Mosaic
6	Cropland/Woodland Mosaic
7	Grassland
8	Shrubland
9	Mixed Shrubland/Grassland
10	Savanna
11	Deciduous Broadleaf Forest
12	Deciduous Needleleaf Forest
13	Evergreen Broadleaf Forest
14	Evergreen Needleleaf Forest
15	Mixed Forest
16	Water
17	Herbaceous Wetland
18	Wooded Wetland
19	Barren or Sparsely Vegetated
20	Herbaceous Tundra
21	Wooded Tundra
22	Mixed Tundra
23	Bare Ground Tundra
24	Snow or Ice

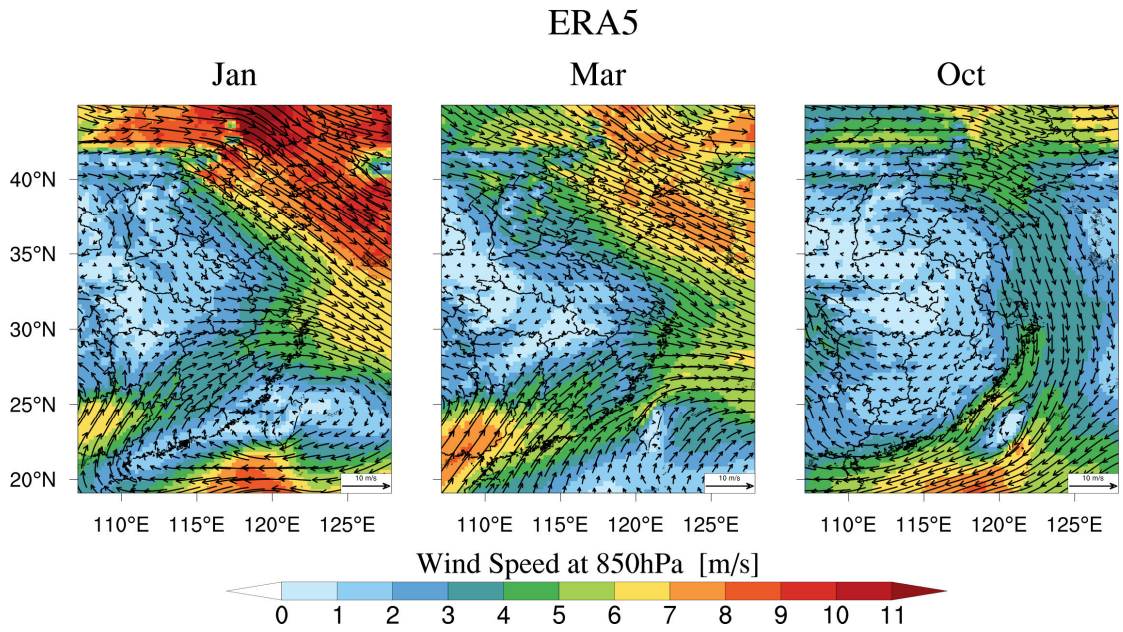

Figure S1. Spatial distribution of wind speeds at 850 hPa from ERA5 reanalysis datasets over East China averaged for January, March, and October of 2019.

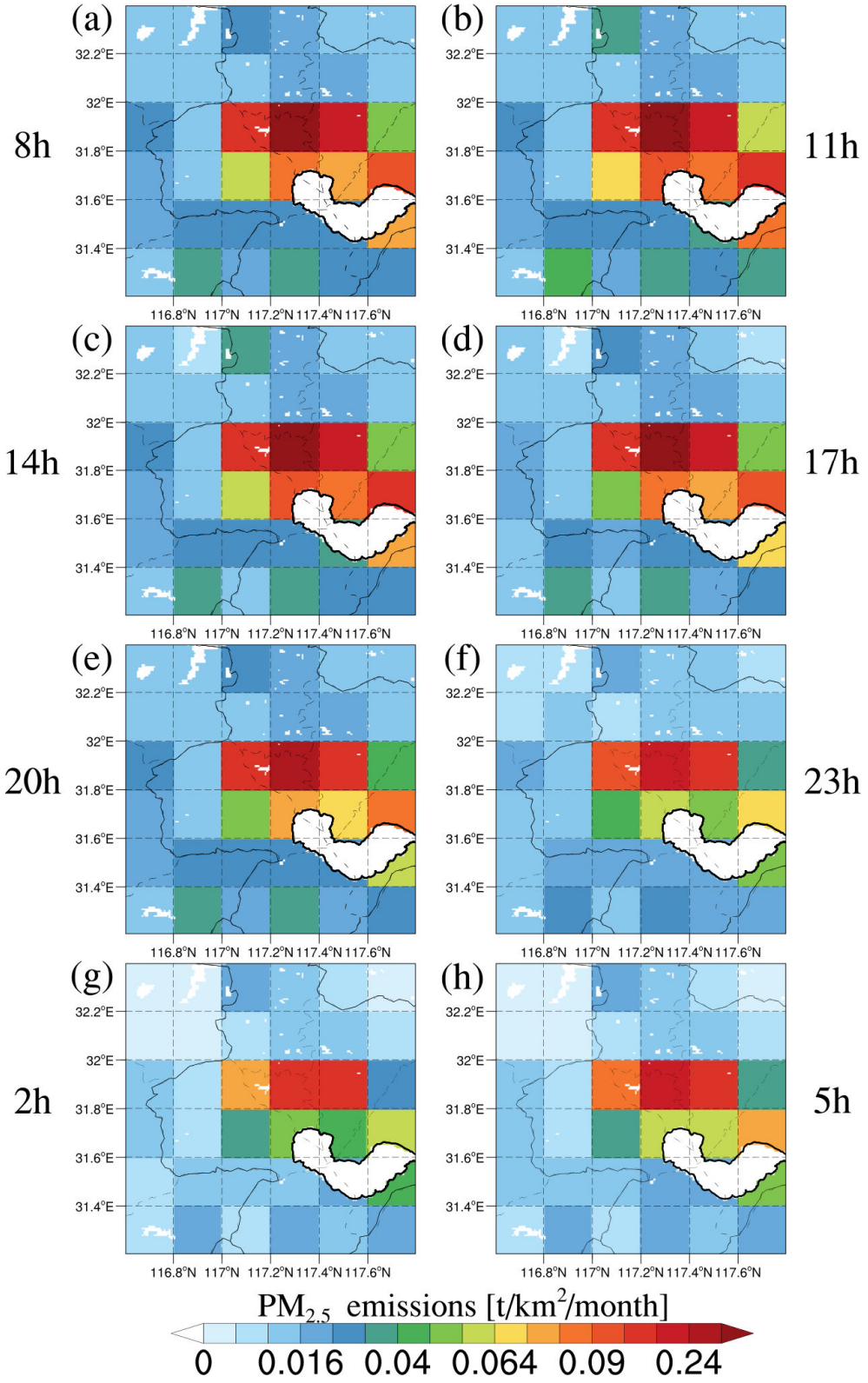

Figure S2. Spatial distribution of $PM_{2.5}$ emissions in both the Lake and Nolake experiments at 08:00, 11:00, 14:00, 17:00, 20:00, 23:00, 02:00, and 05:00 local time (LT), averaged over 10-20 March 2019, throughout the study area.

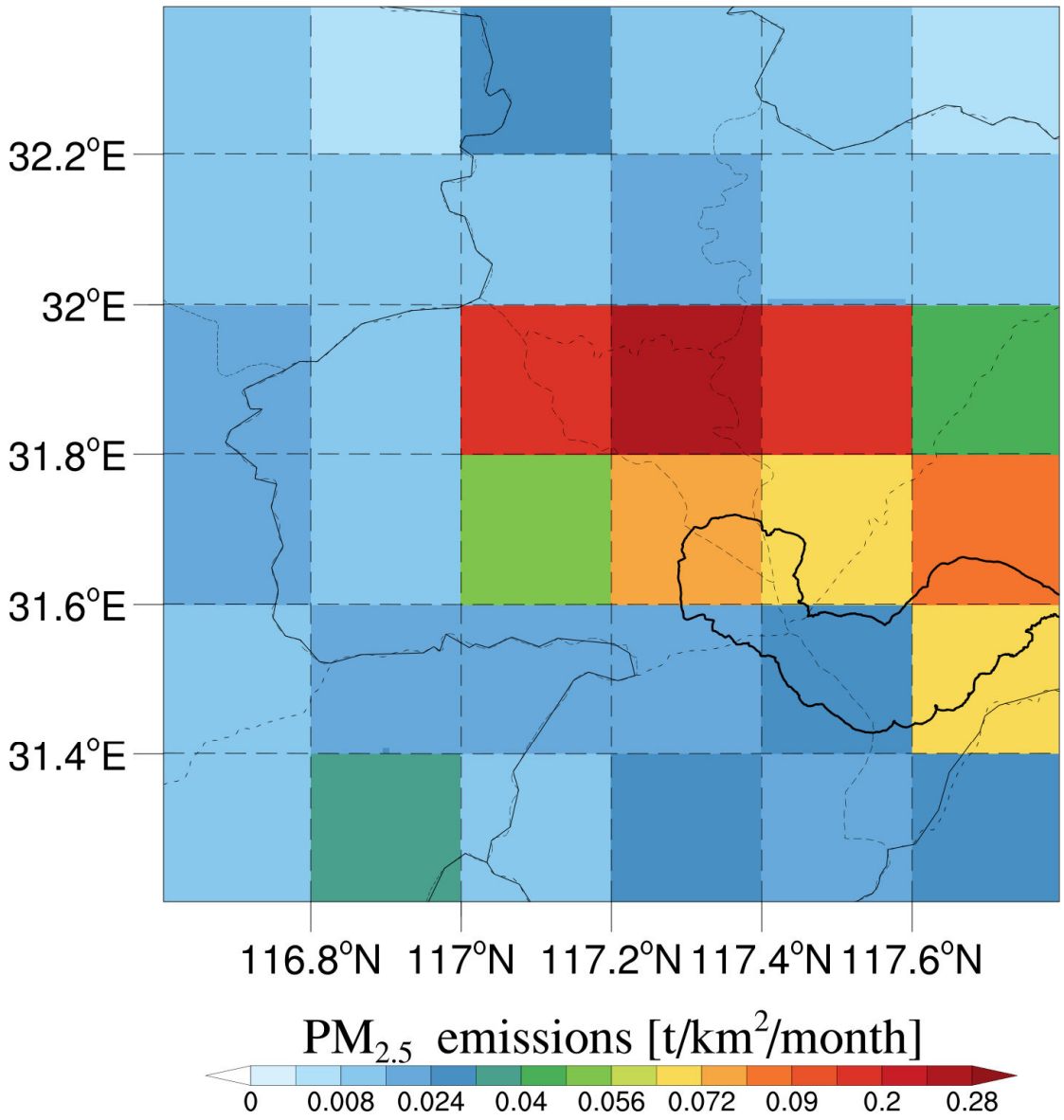

Figure S3. The spatial distribution of $PM_{2.5}$ near-surface emissions in both the Lake_emis and Nolake_emis experiments throughout the study area, averaged over 10-20 March 2019.

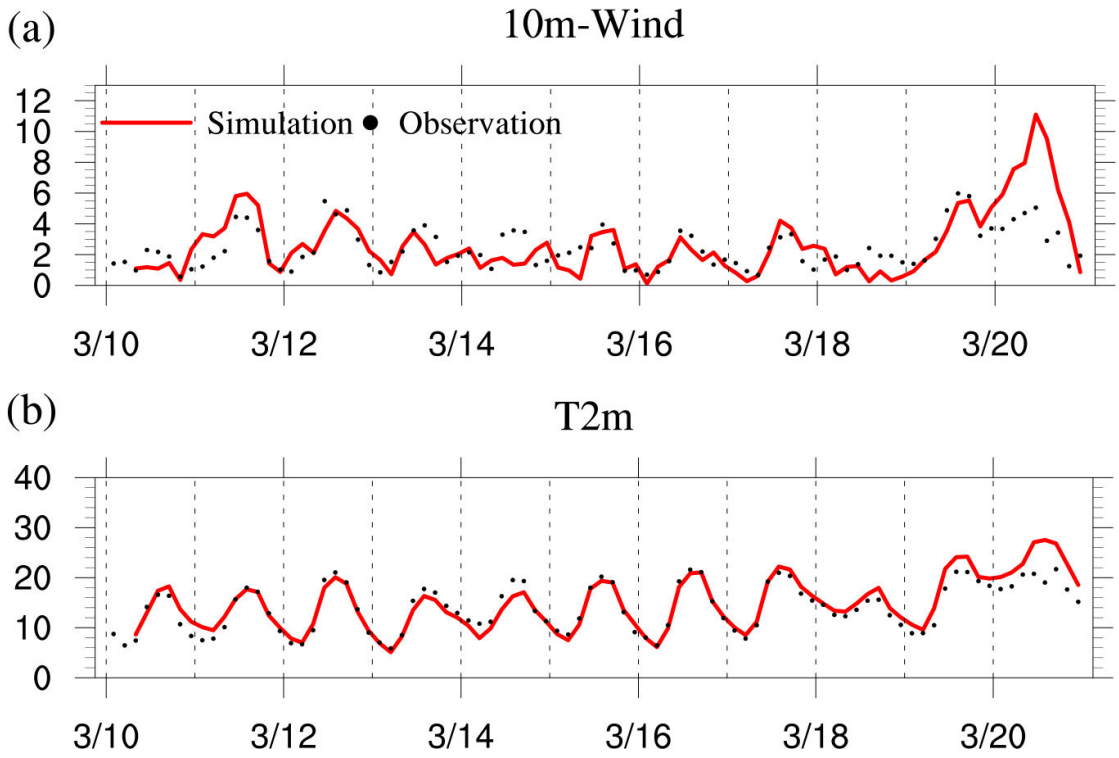

Figure S4. Time series of observed (black dots) and simulated (red line) wind speed at 10 m (top panel, m s^{-1}) and temperature at 2 m (middle panel, °C) from the Lake experiment, averaged over 4 AWS sites in Hefei.

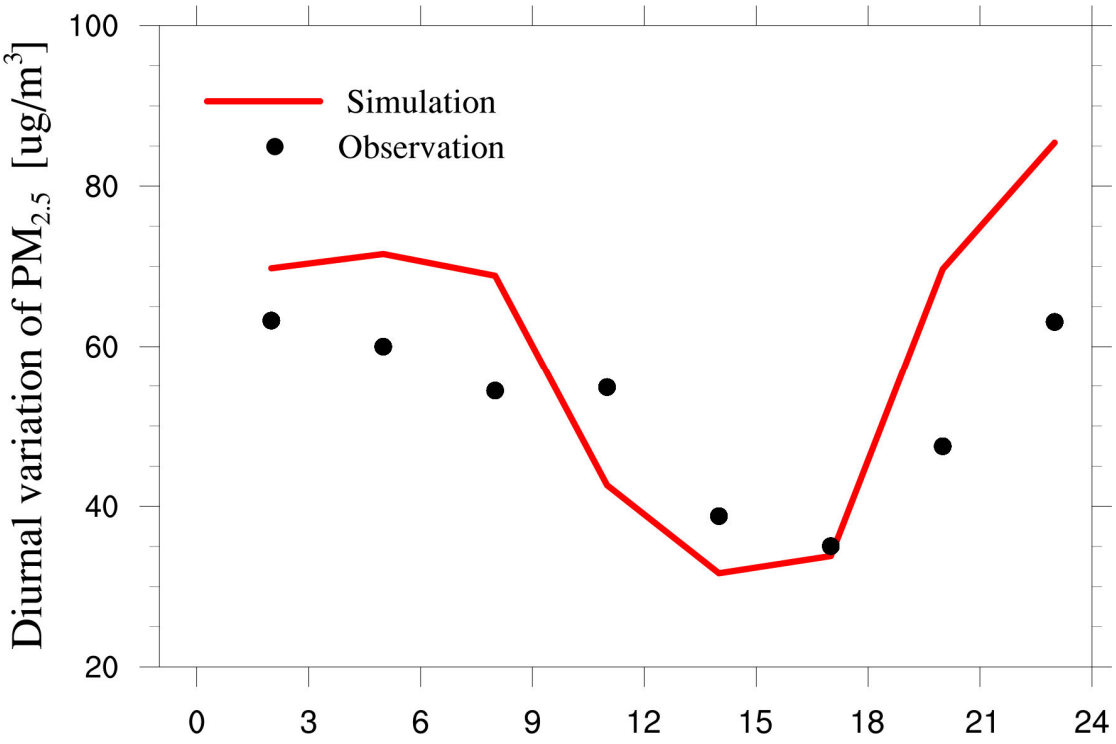

Figure S5. Diurnal variation of $PM_{2.5}$ near-surface concentrations within 24 h averaged over 10 MEP sites in Hefei during the study period for the Lake experiment (solid red line) and observations (black dot). Both the simulated results and observations are sampled at the model output frequency, i.e., 3-hourly.

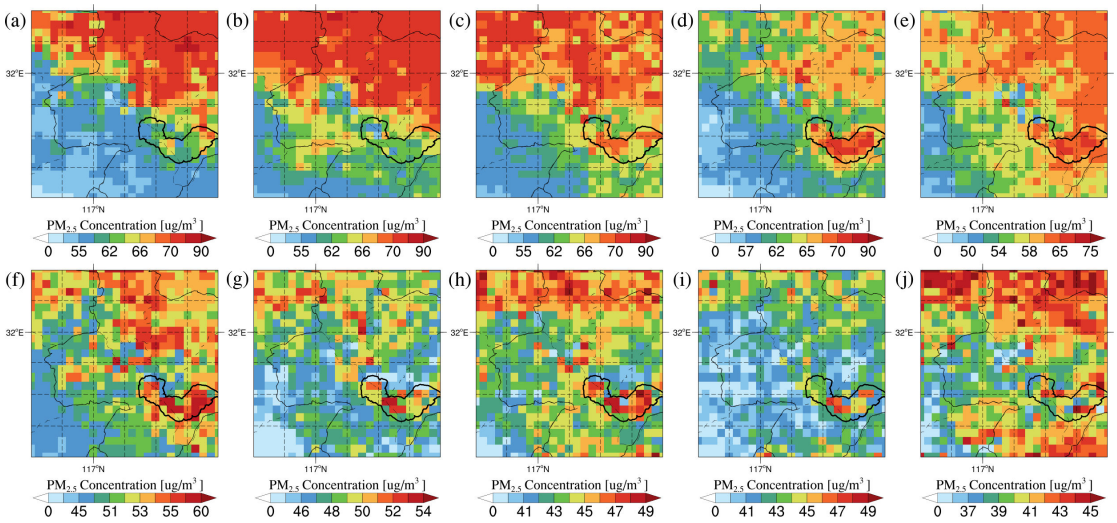

Figure S6. The spatial distribution of $PM_{2.5}$ near-surface concentrations from the ChinaHigh$PM_{2.5}$ dataset (satellite-derived hourly 5 km resolution ground-level $PM_{2.5}$ for Eastern China, 2018) at (a-j) 08:00, 09:00, 10:00, 11:00, 12:00, 13:00, 14:00, 15:00, 16:00, and 17:00 LT across the study area, averaged over the period of March 2018. This dataset belongs to the "Long-term, Seamless, High-resolution, High-quality Dataset of Air Pollutants in China" series (i.e., the "China High Air Pollutants" (CHAP) dataset). The ChinaHigh$PM_{2.5}$ dataset integrates multi-source big data (e.g., ground observation data, satellite remote sensing products, atmospheric reanalysis, and numerical model simulations) using artificial intelligence, fully considering the spatiotemporal heterogeneity characteristics of air pollution.

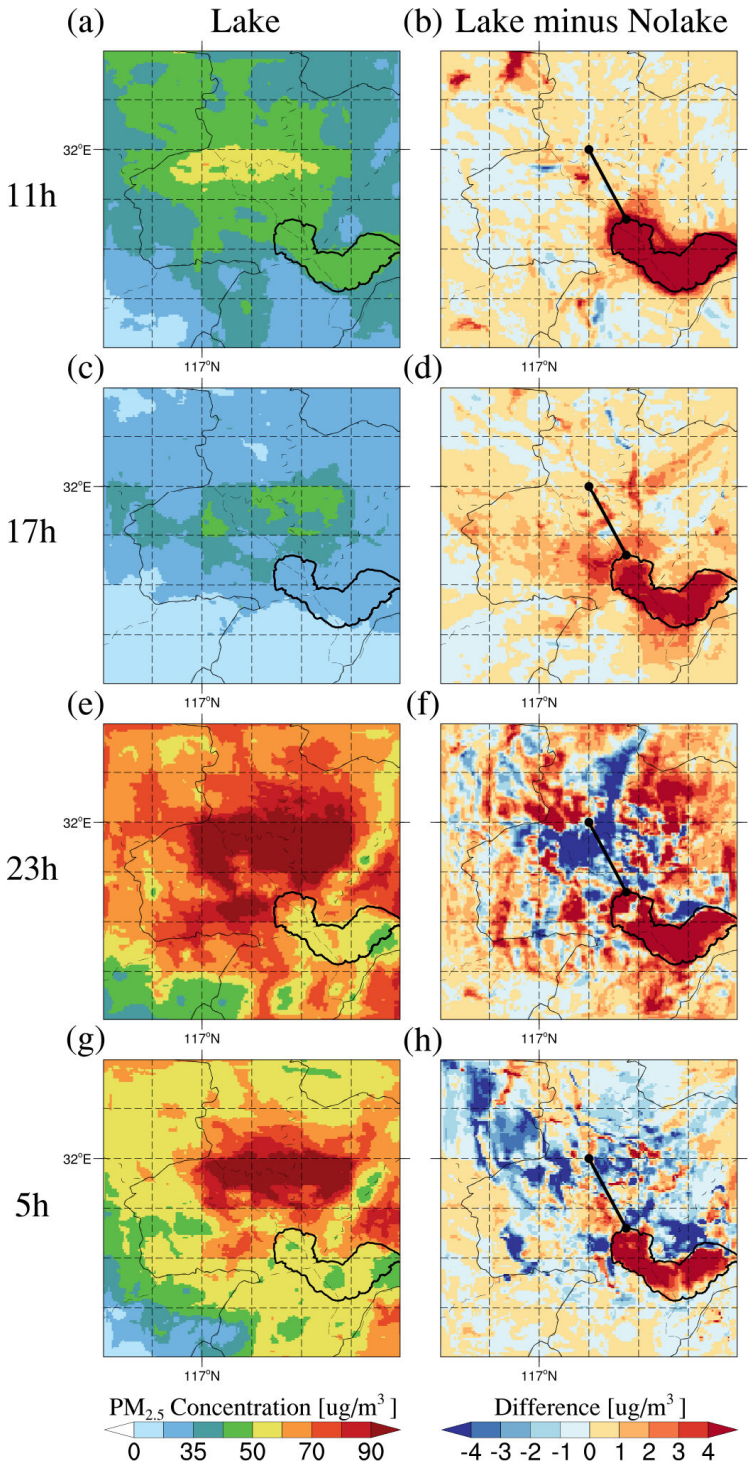

Figure S7. The spatial distribution of $PM_{2.5}$ near-surface concentrations in the (a、c、e、g) Lake experiment and (b、d、f、h) the differences between Lake and Nolake experiments (Lake minus Nolake) at 11:00, 17:00, 23:00, and 05:00 LT across the study area, averaged over 10-20 March 2019. Note that the line segments shown in panels (b, d, f, h) correspond to the AB transect marked in Figure 2.

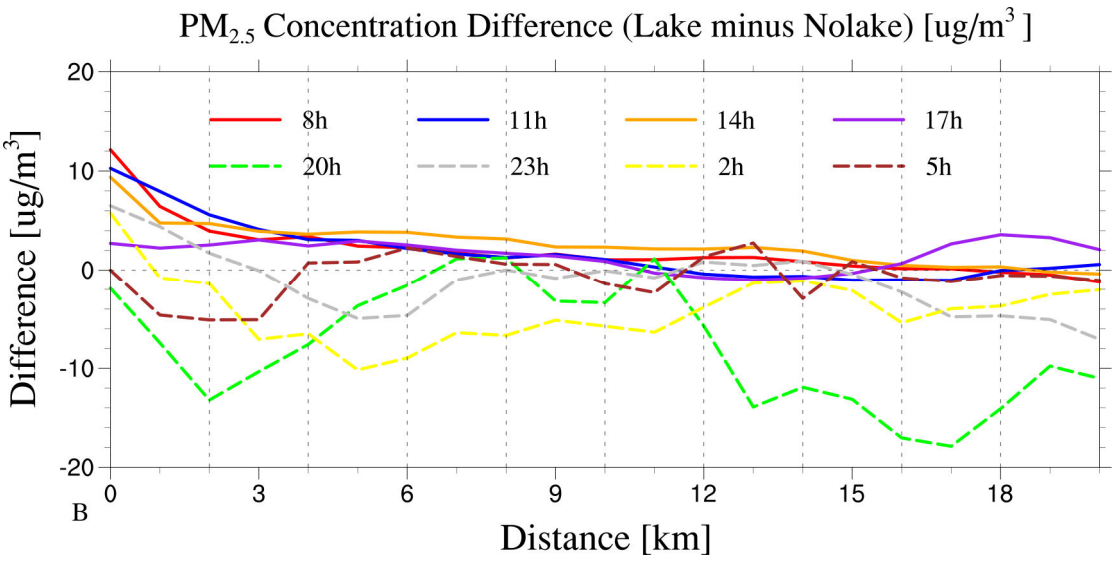

Figure S8. Average $PM_{2.5}$ near-surface concentration differences (Lake minus Nolake) at 08:00, 11:00, 14:00,17:00, 20:00, 23:00, 02:00, and 05:00 LT, averaged over 10-20 March 2019, as a function of distance from point B toward A. The x-axis represents the distance from point B along the path and the y-axisre presents the concentration difference.

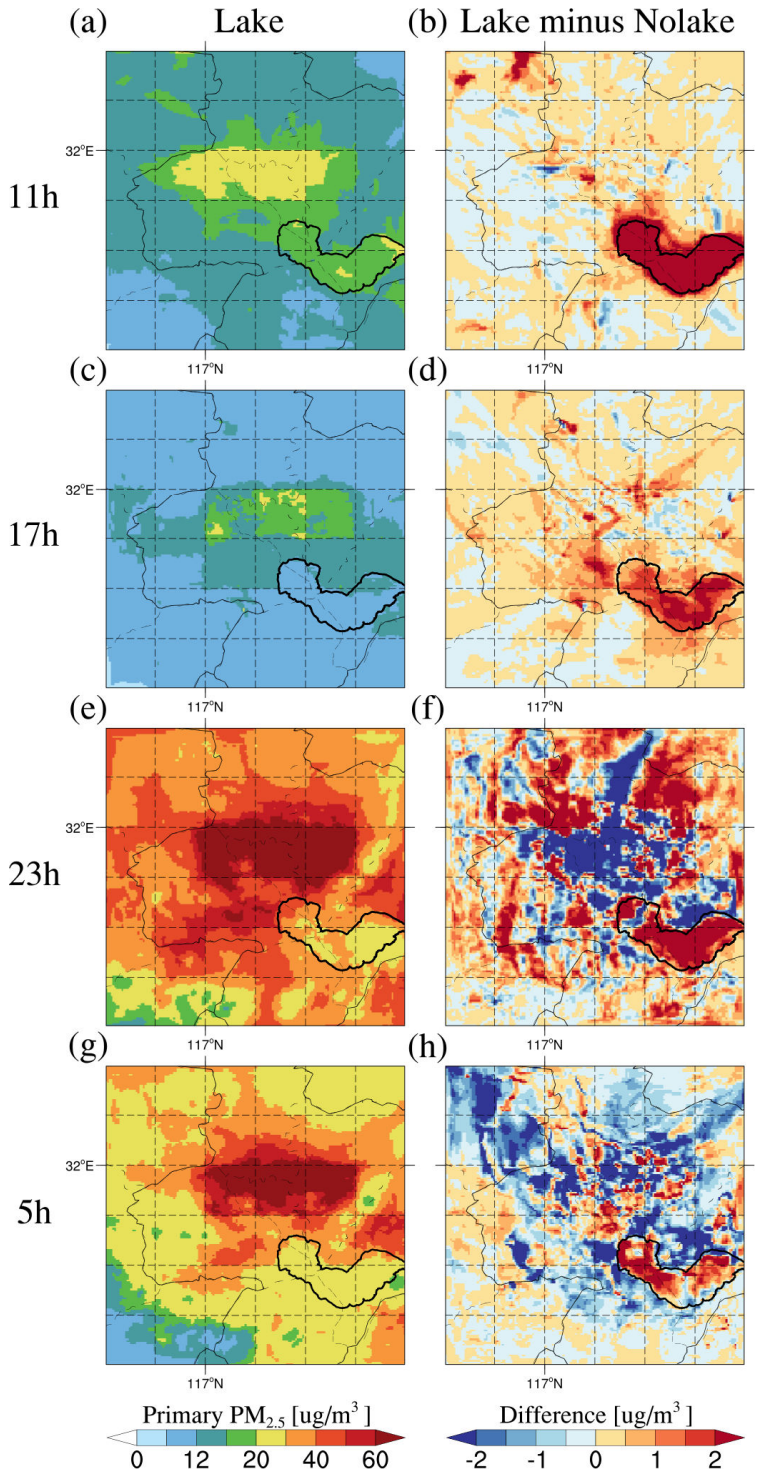

200

201 **Figure S9.** The spatial distribution of primary $PM_{2.5}$ near-surface concentrations (sum
202 of black carbon (BC), organic carbon (OC), and other inorganics (OIN)) in the (a、c、
203 e、g) Lake experiment and (b、d、f、h) the differences between Lake and Nolake
204 experiments (Lake minus Nolake) at 11:00, 17:00, 23:00, and 05:00 LT across the study
205 area, averaged over 10-20 March 2019.

206

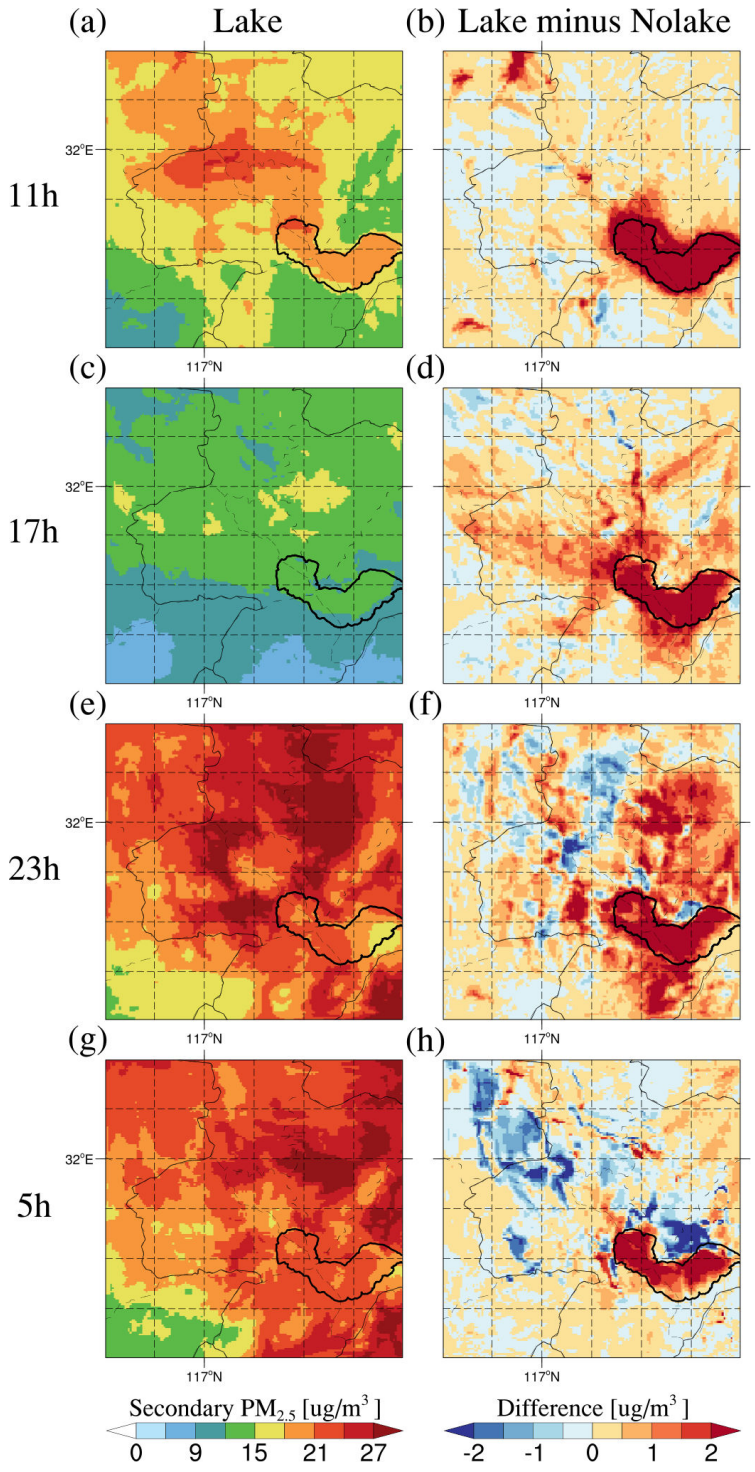

Figure S10. The spatial distribution of secondary $PM_{2.5}$ near-surface concentrations (sum of sulfate (SO_4^{2-}), nitrate (NO_3^-), and ammonium (NH_4^+)) in the (a、c、e、g) Lake experiment and (b、d、f、h) the differences between Lake and Nolake experiments (Lake minus Nolake) at 11:00, 17:00, 23:00, and 05:00 LT across the study area, averaged over 10-20 March 2019.

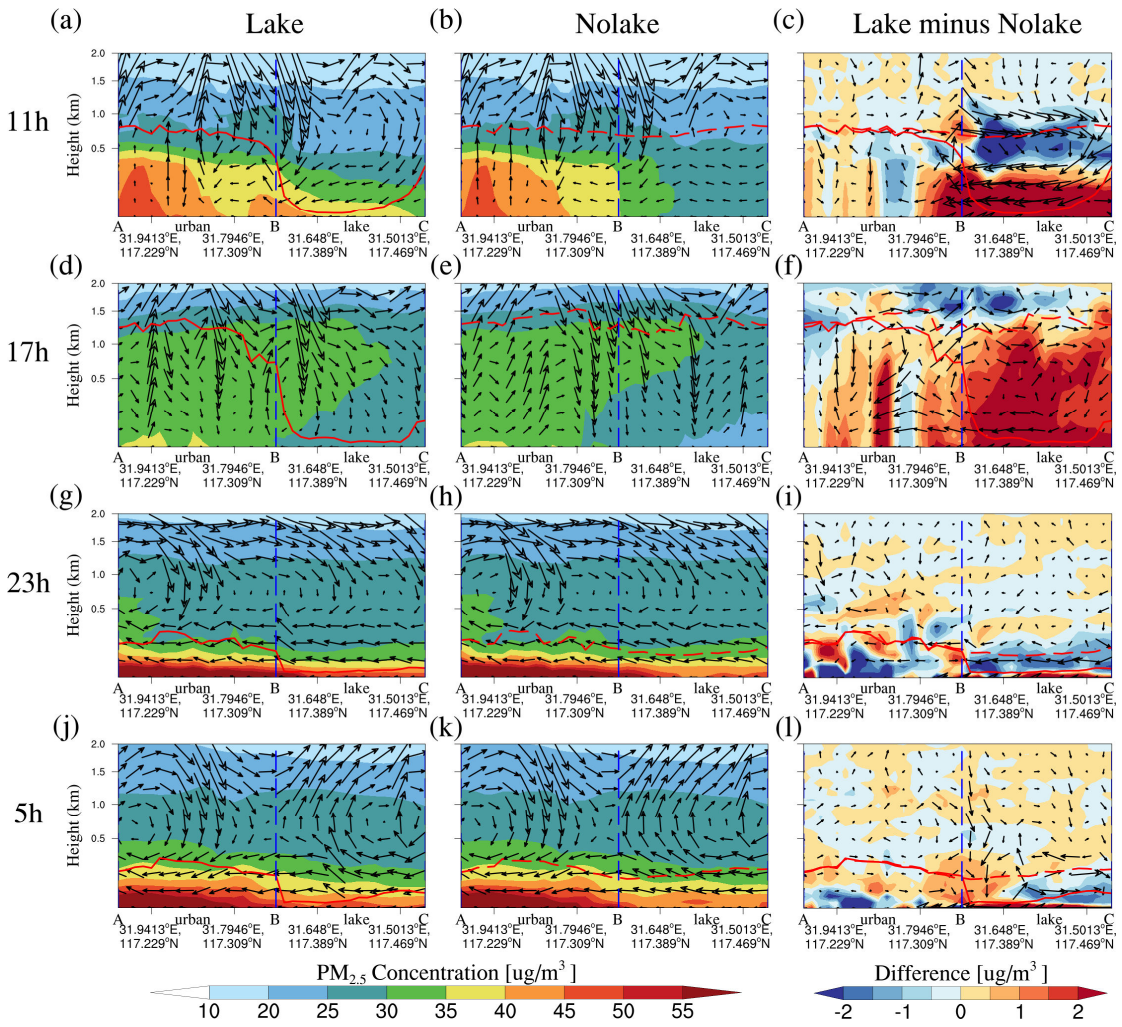

Figure S11. The vertical cross-section of $PM_{2.5}$ concentration and wind vectors along the key path AC (indicated in Figure 2) for the (a、d、g、j) Lake experiment, (b、e、h、k) Nolake experiment, and (c、f、i、l) their differences (Lake minus Nolake) at 11:00, 17:00, 23:00, and 05:00 LT, averaged over 10-20 March 2019. The shaded contours represent $PM_{2.5}$ concentrations or their differences between the two experiments at each altitude. The black vector arrows indicate the superimposed vertical wind field (including horizontal and vertical wind components), with the vertical wind vector being multiplied by 50 for visibility. The red solid line represents the planetary boundary layer height (PBLH) in the Lake experiment, and the red dashed line represents the PBLH in the Nolake experiment. The blue dashed line represents the lake-land boundary.

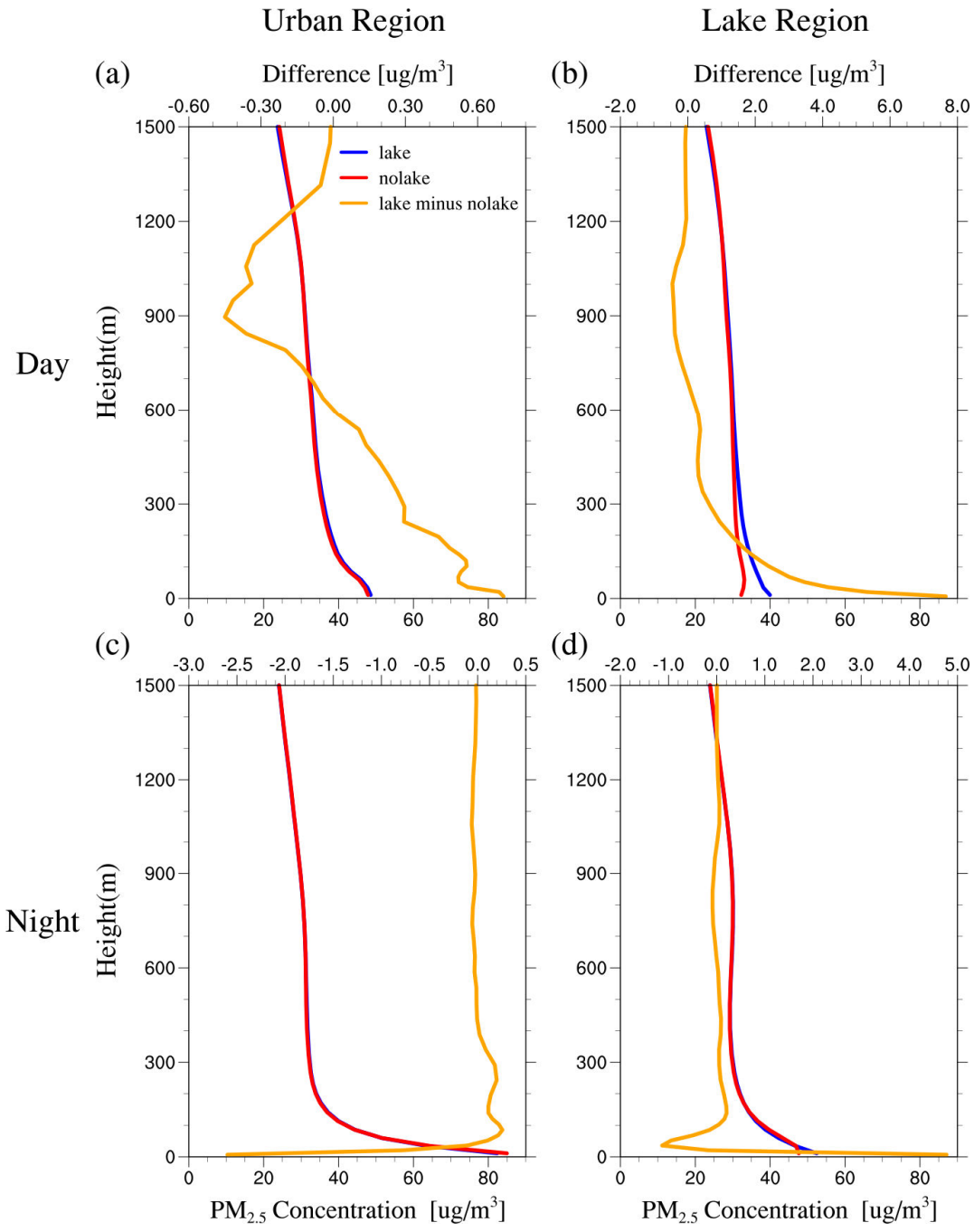

228

229 **Figure S12.** The vertical profiles of $PM_{2.5}$ concentrations simulated in the Lake
230 experiment (solid blue line), Nolake experiment (solid red line), and their differences
231 (Lake minus Nolake, solid orange line) over (a, c) urban and (b, d) lake regions during
232 daytime and nighttime, averaged over 10-20 March 2019. Note that "Urban Region"
233 represents the average value for areas with urban underlying surface within the study
234 domain, while "Lake Region" represents the average value for areas with lake
235 underlying surface within the study domain, to make the results more representative.

236

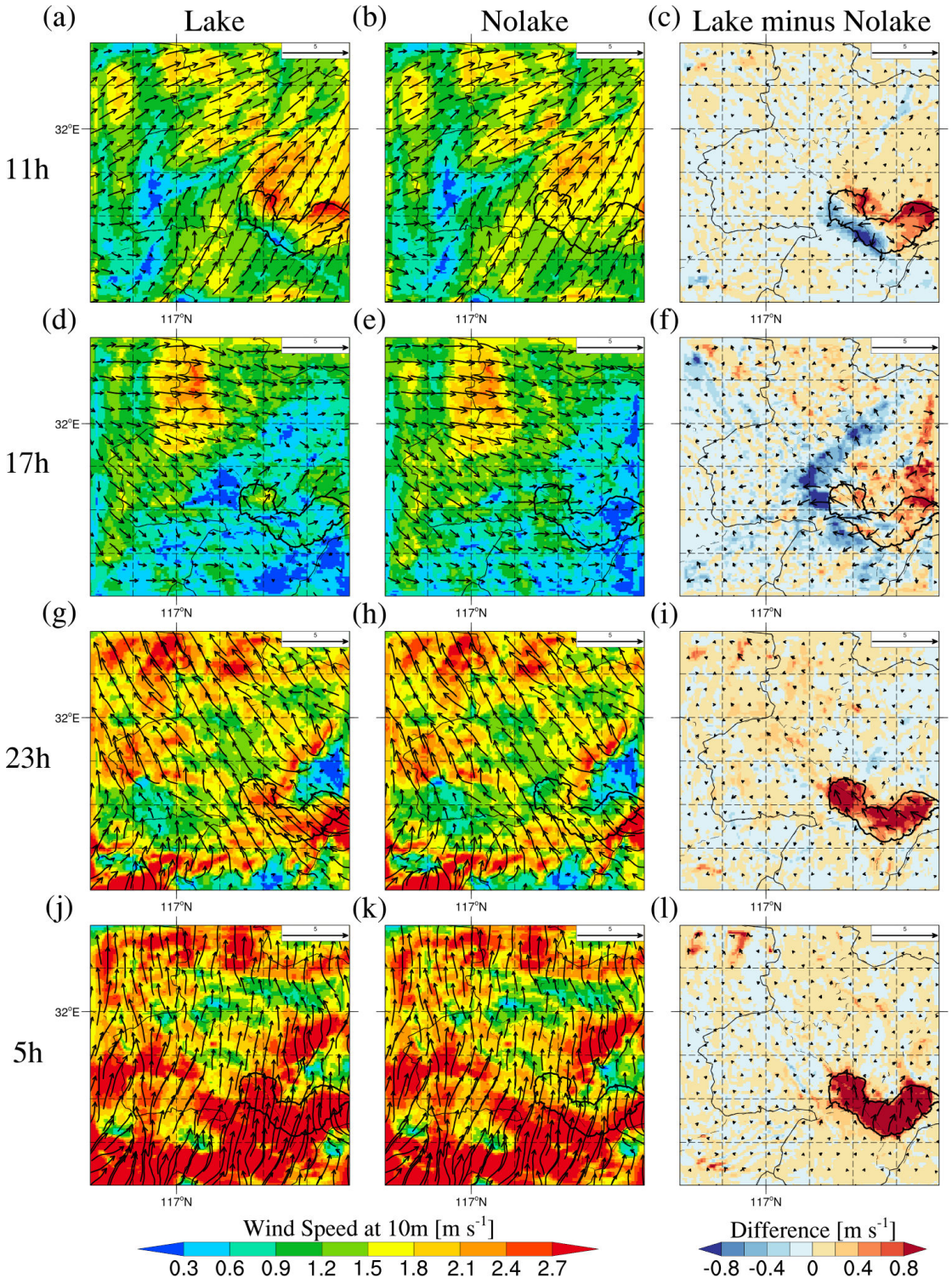

Figure S13. The spatial distribution of 10-m wind speed in the (a、d、g、j) Lake experiment, (b、e、h、k) Nolake experiment, and (c、f、i、l) their differences (Lake minus Nolake) at 11:00, 17:00, 23:00, and 05:00 LT across the study area, averaged over 10-20 March 2019.

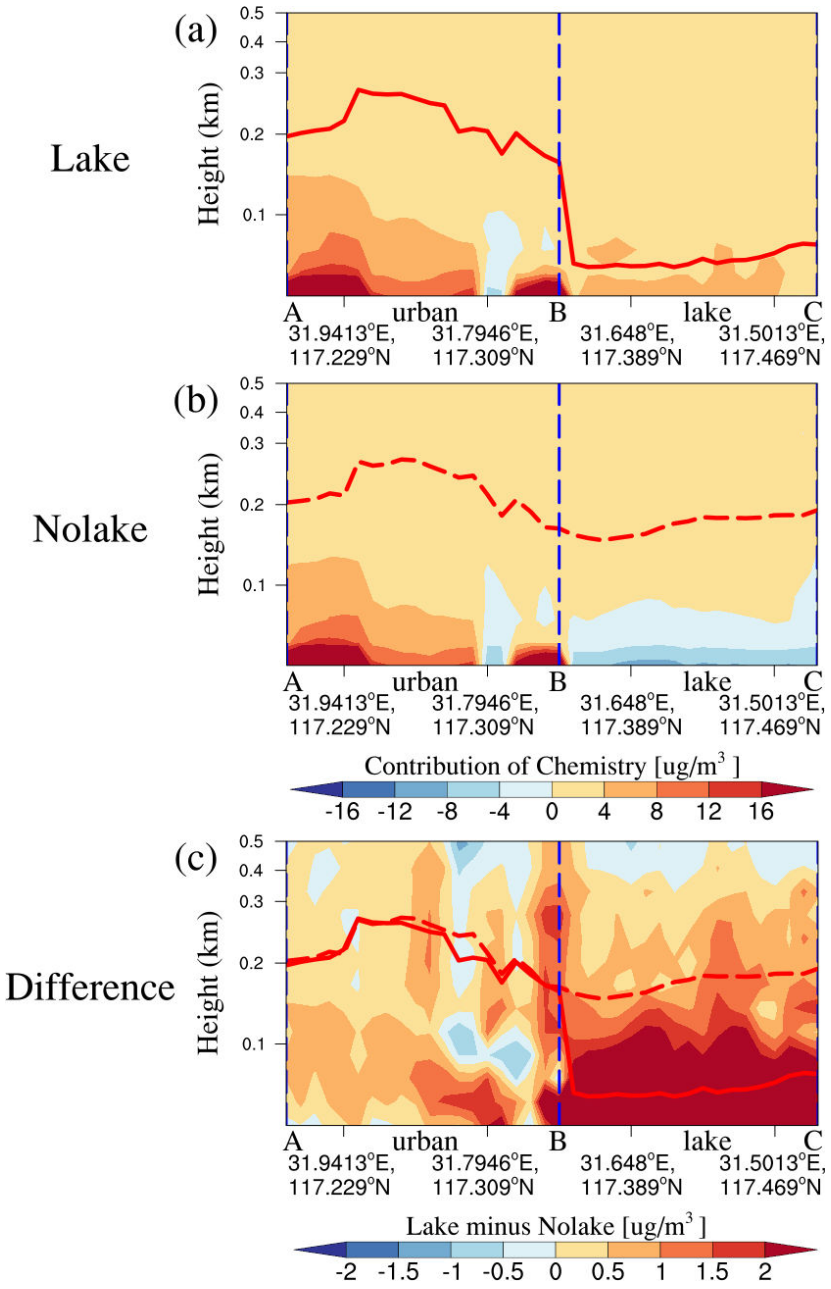

Figure S14. The vertical cross-section of chemical process contributions to $PM_{2.5}$ concentrations along the key path AC (indicated in Figure 2) for the (a) Lake experiment, (b) Nolake experiment, and (c) their differences (Lake minus Nolake) during nighttime, averaged over 10-20 March 2019. The shaded contours represent the contribution of chemical processes to surface $PM_{2.5}$ concentrations or their differences between the two experiments at each altitude. The red solid line represents the PBLH in the Lake experiment, and the red dashed line represents the PBLH in the Nolake experiment. The blue dashed line represents the lake-land boundary.

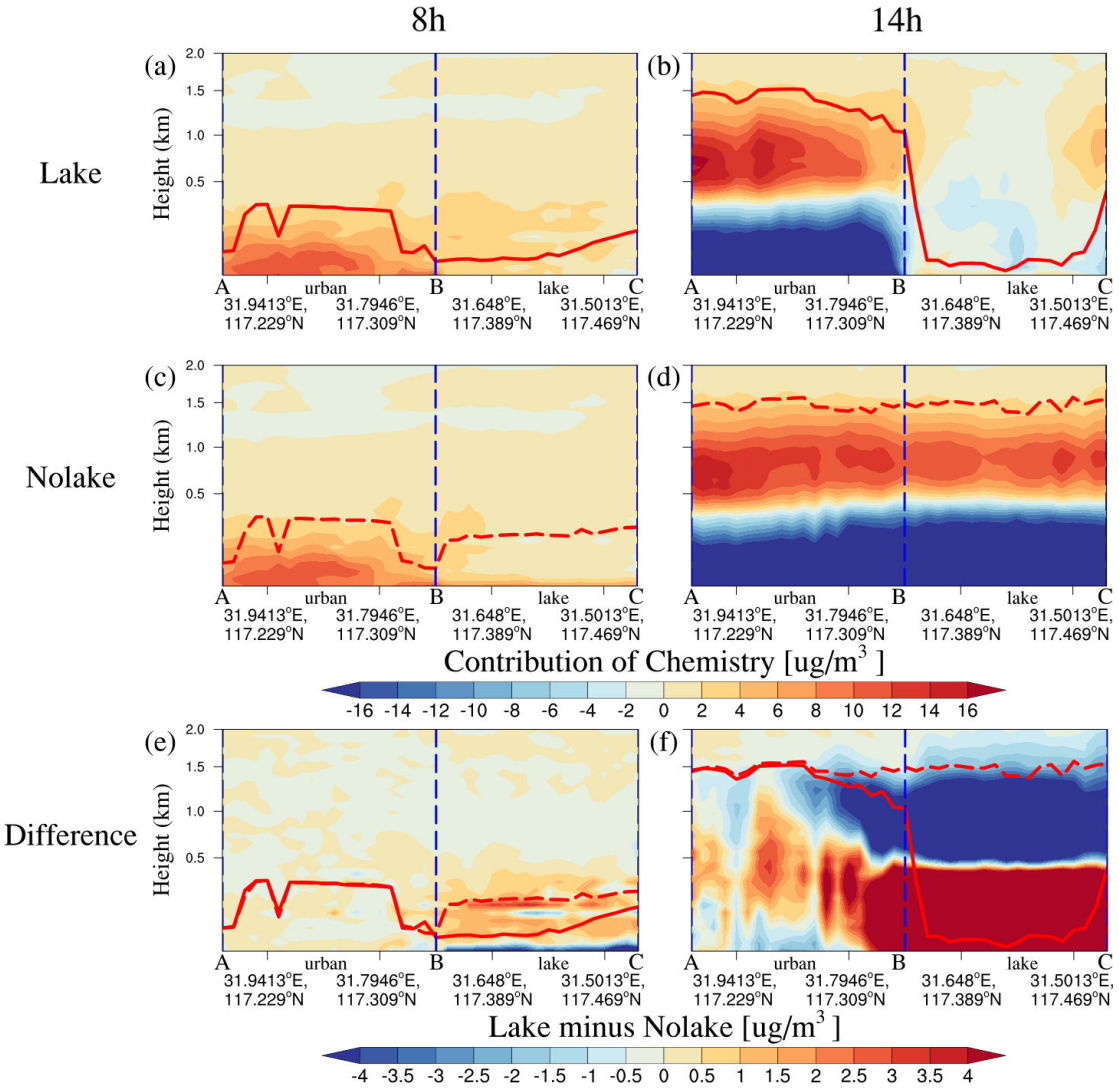

Figure S15. The vertical cross-section of chemical process contributions to $PM_{2.5}$ concentrations along the key path AC (indicated in Figure 2) for the (a、b) Lake experiment, (c、d) Nolake experiment, and (e、f) their differences (Lake minus Nolake) at 08:00 and 14:00 LT, averaged over 10-20 March 2019. The shaded contours represent the contribution of chemical processes to surface $PM_{2.5}$ concentrations or their differences between the two experiments at each altitude. The red solid line represents the planetary boundary layer height (PBLH) in the Lake experiment, and the red dashed line represents the PBLH in the Nolake experiment. The blue dashed line represents the lake-land boundary.

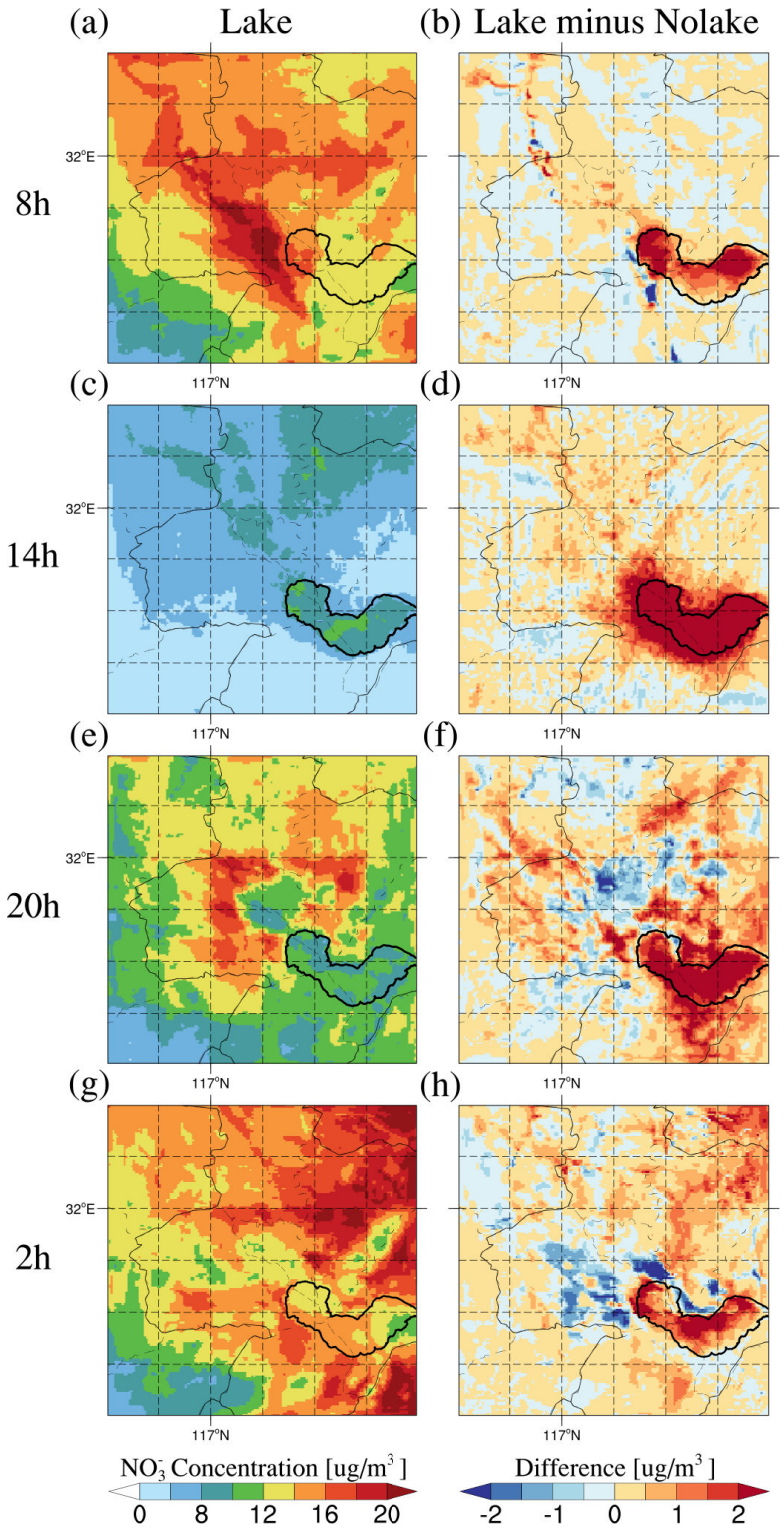

Figure S16. The spatial distribution of NO_3^- near-surface concentrations in the (a、c、e、g) Lake experiment and (b、d、f、h) the differences between Lake and Nolake experiments (Lake minus Nolake) at 08:00, 14:00, 20:00, and 02:00 LT across the study area, averaged over 10-20 March 2019.

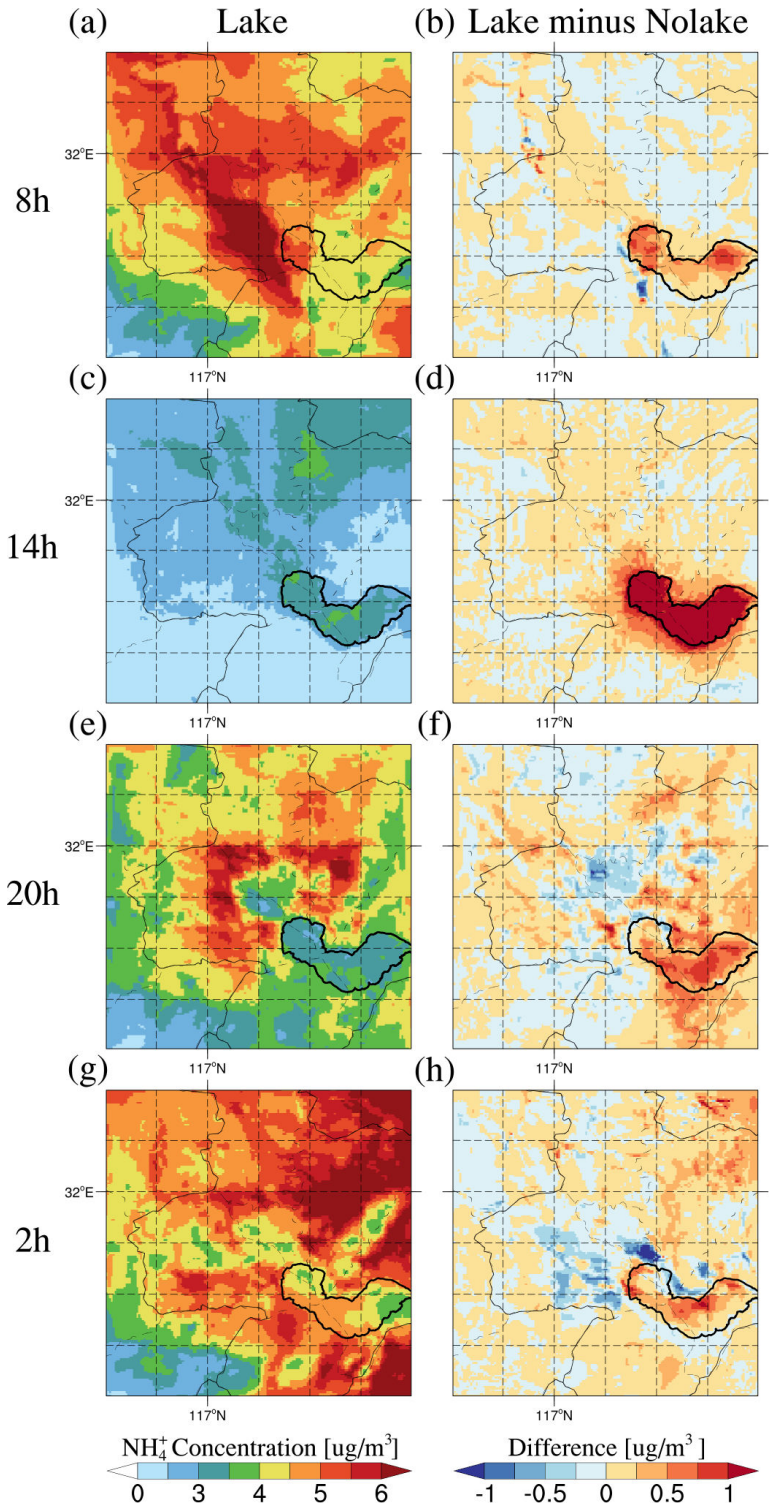

Figure S17. The spatial distribution of NH_4^+ near-surface concentrations in the (a、c、e、g) Lake experiment and (b、d、f、h) the differences between Lake and Nolake experiments (Lake minus Nolake) at 08:00, 14:00, 20:00, and 02:00 LT across the study area, averaged over 10-20 March 2019.

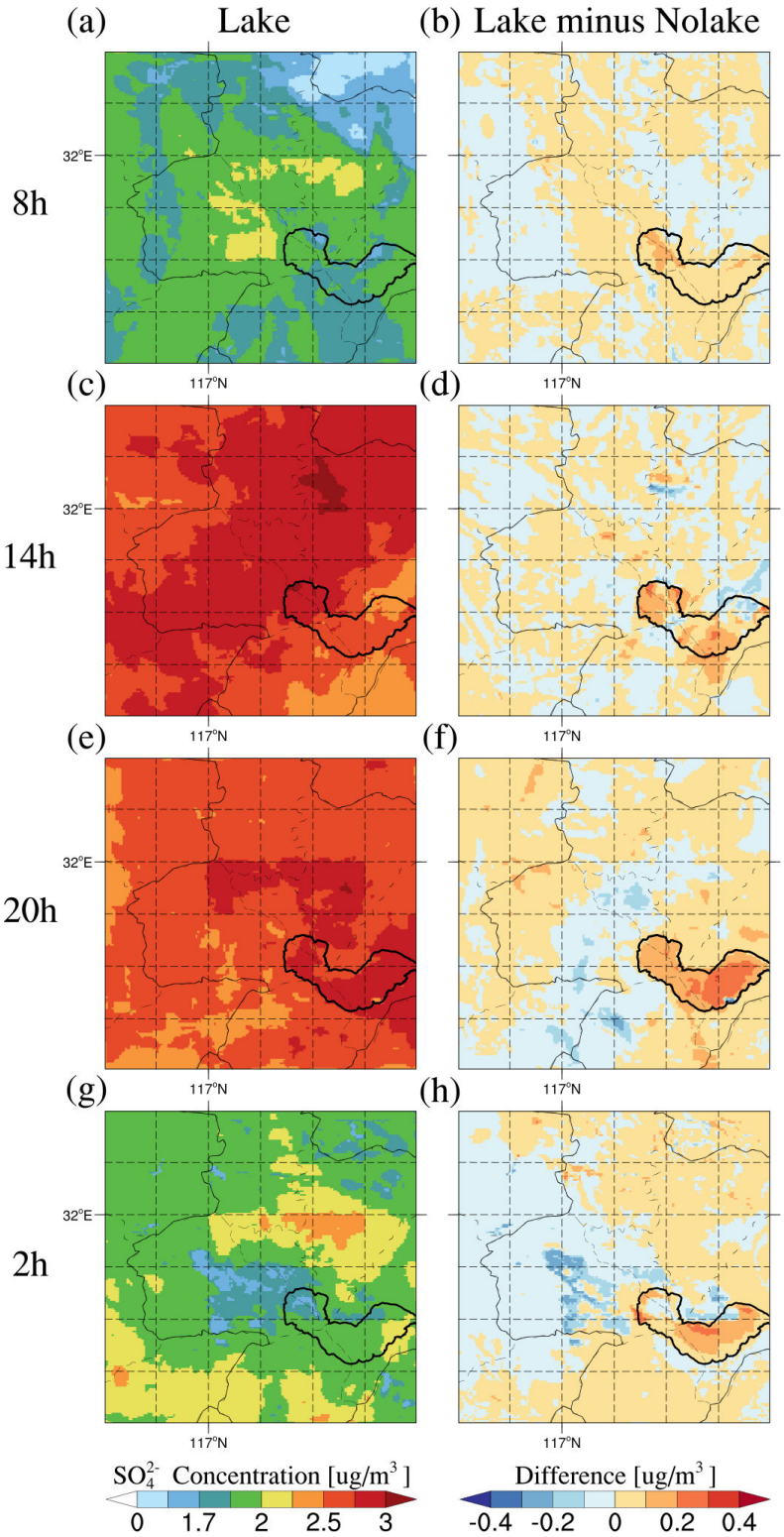

277

278 **Figure S18.** The spatial distribution of SO_4^{2-} near-surface concentrations in the (a、c、

279 e、g) Lake experiment and (b、d、f、h) the differences between Lake and Nolake

280 experiments (Lake minus Nolake) at 08:00, 14:00, 20:00, and 02:00 LT across the study

281 area, averaged over 10-20 March 2019.

282

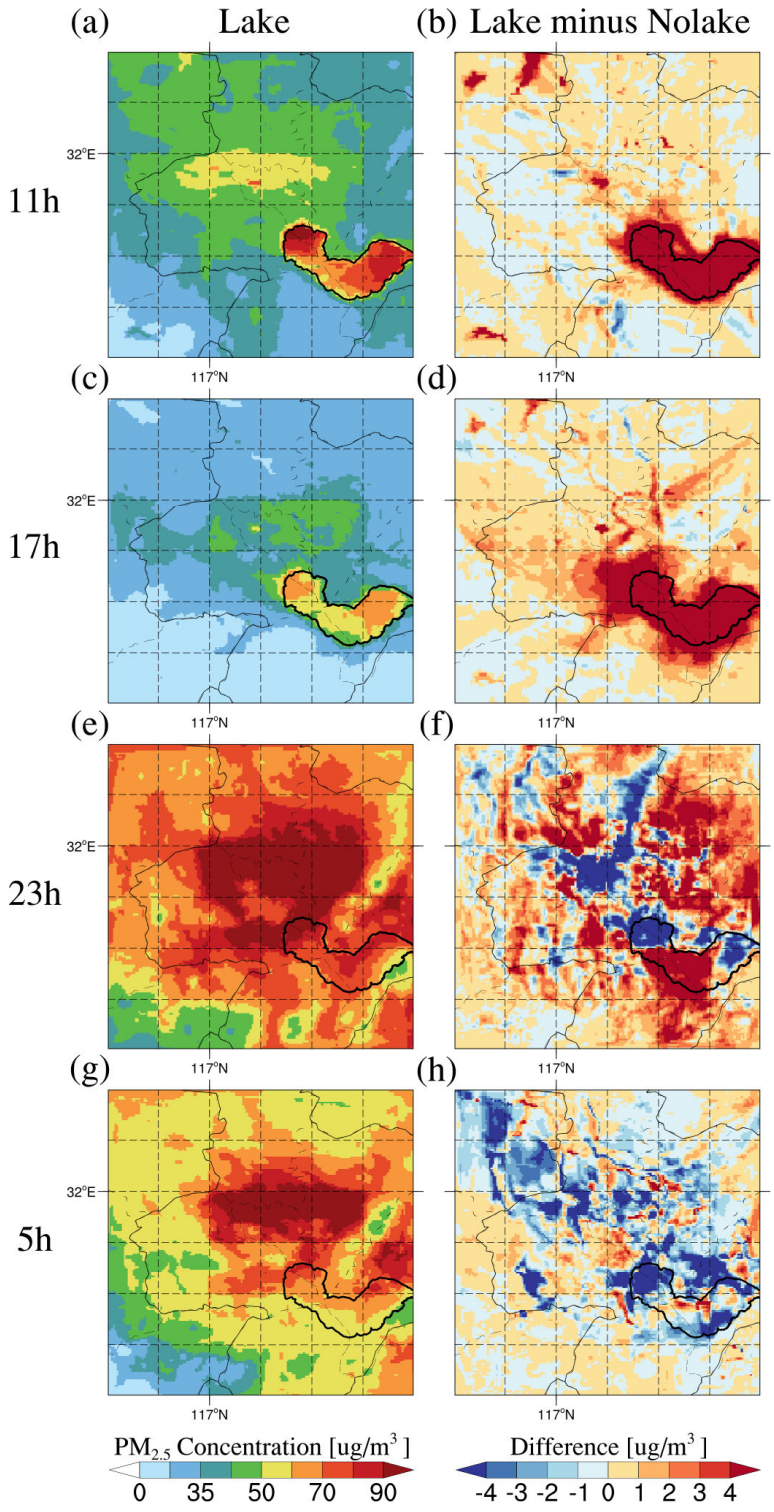

Figure S19. The spatial distribution of $PM_{2.5}$ near-surface concentrations in the (a、c、e、g) Lake_emis experiment and (b、d、f、h) the differences between Lake_emis and Nolake_emis experiments (Lake_emis minus Nolake_emis) at 11:00, 17:00, 23:00, and 05:00 LT across the study area, averaged over 10-20 March 2019.

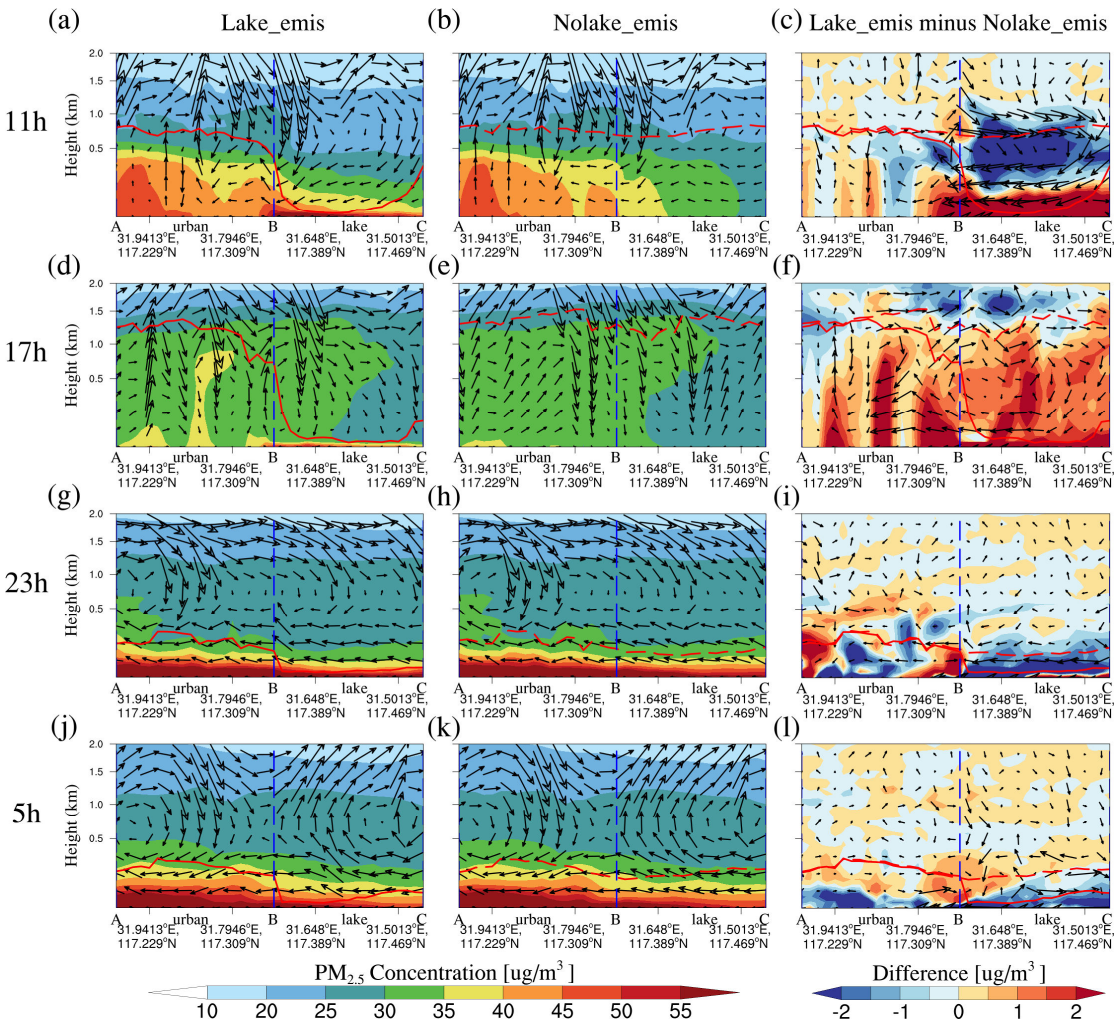

Figure S20. The vertical cross-section of $PM_{2.5}$ concentration and wind vectors along the key path AC (indicated in Figure 2) for the (a、d、g、j) Lake_emis experiment, (b、e、h、k) Nolake_emis experiment, and (c、f、i、l) their differences (Lake_emis minus Nolake_emis) at 11:00, 17:00, 23:00, and 05:00 LT, averaged over 10-20 March 2019. The shaded contours represent $PM_{2.5}$ concentrations or their differences between the two experiments at each altitude. The black vector arrows indicate the superimposed vertical wind field (including horizontal and vertical wind components), with the vertical wind vector being multiplied by 50 for visibility. The red solid line represents the planetary boundary layer height (PBLH) in the Lake experiment, and the red dashed line represents the PBLH in the Nolake experiment. The blue dashed line represents the lake-land boundary.